Article
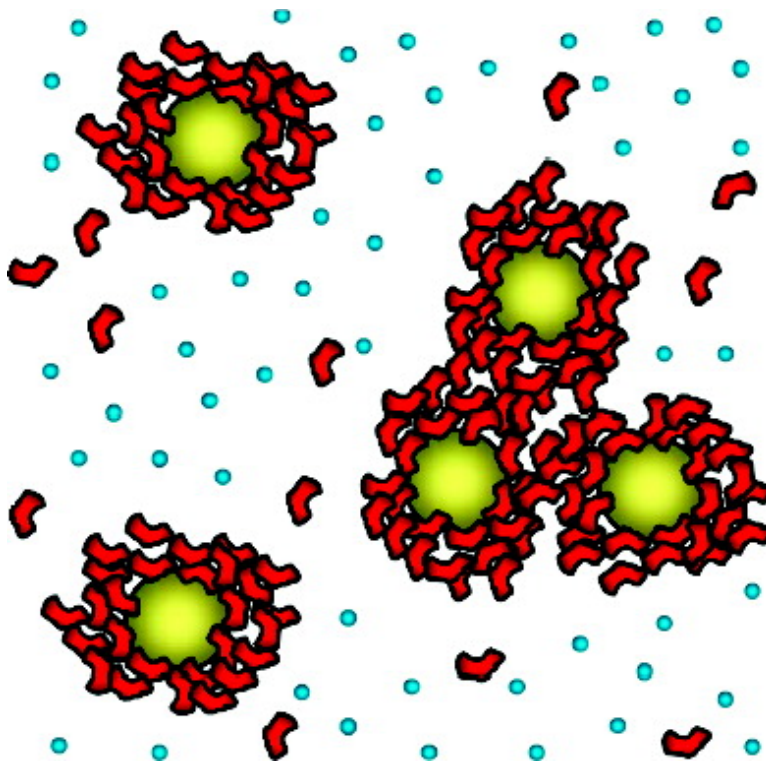
Self-Interaction Nanoparticle Spectroscopy: A Nanoparticle-Based Protein Interaction Assay

Peter M. Tessier, Jun Jinkoji, Yu-Chia Cheng, Jessica L. Prentice, and Abraham M. Lenhoff

More About This Article

Additional resources and features associated with this article are available within the HTML version:

- Supporting Information
- Access to high resolution figures
- Links to articles and content related to this article
- Copyright permission to reproduce figures and/or text from this article

Self-Interaction Nanoparticle Spectroscopy: A Nanoparticle-Based Protein Interaction Assay

Peter M. Tessier,*,† Jun Jinkoji, Yu-Chia Cheng, Jessica L. Prentice, and Abraham M. Lenhoff

Center for Molecular and Engineering Thermodynamics, Department of Chemical Engineering, University of Delaware, Newark, Delaware 19716

Received October 12, 2007; E-mail: tessier@rpi.edu

Abstract: Solution conditions conducive to protein crystallization are identified mainly in an empirical manner using screening methods. Measurements of a dilute solution thermodynamic parameter, the osmotic second virial coefficient, have been shown to be useful in guiding this search, yet the measurement of this parameter remains difficult. In this work, a nanoparticle-based assay, self-interaction nanoparticle spectroscopy, is presented as an efficient alternative. The method involves adsorbing proteins on the surface of gold nanoparticles and adding the protein/gold conjugates to solutions of interest for crystallization. The optical properties of gold colloid, including macroscopic ones such as color, are sensitive to the interparticle separation distance, and they are demonstrated to correlate with the value of the second virial coefficient for BSA and ovalbumin. Serendipitously, the conditions that correspond to second virial coefficient values within the thermodynamic region ideal for protein crystallization lead to the maximum change in color of the gold suspensions. Given the remarkable efficiency of this method, it holds significant potential to aid in the crystallization of proteins that have not been crystallized previously. Moreover, this method may find utility in the analysis of weak homo- and heterotypic interactions involved in other biological applications, including preventing protein aggregation and formulating therapeutic proteins.

Introduction

The importance of detailed protein structural information obtained by X-ray diffraction of protein crystals has led to a significant amount of research in the area of protein self-assembly. A particularly important finding in this area has been that weakly attractive protein interactions, characterized in terms of slightly negative values of the osmotic second virial coefficient (B_{22}), correlate with solution conditions that are conducive to crystallization, while repulsive (positive B_{22} values) or strongly attractive (large negative B_{22} values) protein interactions lead to no phase separation or precipitation, respectively.[1] This region of slightly negative B_{22} values, -1 to -8×10^{-4} mol-mL/g^2, was named the "crystallization slot", and its existence has been confirmed by a number of studies.[2–8] However, the lack of robust techniques for measuring B_{22} has proven to be a significant barrier to the practical implementation of using B_{22} values as a guide to crystallizing proteins that have not been crystallized previously.

Traditional techniques for measuring B_{22} include static light scattering (SLS),[1–3,5] membrane osmometry,[9,10] small-angle X-ray[11,12] and neutron[4,13] scattering, sedimentation equilibrium[14] and size-exclusion chromatography.[15,16] All of these techniques suffer from poor efficiency in terms of time and protein consumption. For example, traditional SLS requires about 25 mg of protein and several hours per B_{22} value. Recently, there have been several new or improved methods proposed for measuring B_{22}, including self-interaction chromatography,[17,18] as well as more efficient forms of SLS[19] and size-exclusion chromatography,[15] some of which have demonstrated improve-

† Current address: Center for Biotechnology and Interdisciplinary Studies, Howard P. Isermann Department of Chemical and Biological Engineering, Rensselaer Polytechnic Institute, Troy, NY 12180.

(1) George, A.; Wilson, W. W. *Acta Crystallogr. D* **1994**, *50*, 361–365.
(2) Guo, B.; Kao, S.; McDonald, H.; Asanov, A.; Combs, L. L.; Wilson, W. W. *J. Cryst. Growth* **1999**, *196*, 424–433.
(3) Bonneté, F.; Finet, S.; Tardieu, A. *J. Cryst. Growth* **1999**, *196*, 403–414.
(4) Velev, O. D.; Kaler, E. W.; Lenhoff, A. M. *Biophys. J.* **1998**, *75*, 2682–2697.
(5) Hitscherich, C.; Kaplan, J.; Allaman, M.; Wiencek, J.; Loll, P. J. *Protein Sci.* **2000**, *9*, 1559–1566.
(6) Tessier, P. M.; Johnson, H. R.; Pazhianur, R.; Berger, B. W.; Prentice, J. L.; Bahnson, B. J.; Sandler, S. I.; Lenhoff, A. M. *Proteins* **2003**, *50*, 303–311.
(7) Rosenbaum, D.; Zamora, P. C.; Zukoski, C. F. *Phys. Rev. Lett.* **1996**, *76*, 150–153.
(8) Petsev, D. N.; Vekilov, P. G. *Phys. Rev. Lett.* **2000**, *84*, 1339–1342.
(9) Schaink, H. M.; Smit, J. A. M. *Phys. Chem. Chem. Phys.* **2000**, *2*, 1537–1541.
(10) Haynes, C. A.; Tamura, K.; Korfer, H. R.; Blanch, H. W.; Prausnitz, J. M. *J. Phys. Chem.* **1992**, *96*, 905–912.
(11) Ducruix, A.; Guilloteau, J. P.; Ries-Kautt, M.; Tardieu, A. *J. Cryst. Growth* **1996**, *168*, 28–39.
(12) Porschel, H. V.; Damaschun, G. *Stud. Biophys.* **1977**, *62*, 69–69.
(13) Receveur, V.; Durand, D.; Desmadril, M.; Calmettes, P. *Febs. Lett.* **1998**, *426*, 57–61.
(14) Behlke, J.; Ristau, O. *Biophys. Chem.* **1999**, *76*, 13–23.
(15) Bloustine, J.; Berejnov, V.; Fraden, S. *Biophys. J.* **2003**, *85*, 2619–2623.
(16) Nichol, L. W.; Siezen, R. J.; Winzor, D. J. *Biophys. Chem.* **1978**, *9*, 47–55.
(17) Patro, S. Y.; Przybycien, T. M. *Biotechnol. Bioeng.* **1996**, *52*, 193–203.
(18) Tessier, P. M.; Lenhoff, A. M.; Sandler, S. I. *Biophys. J.* **2002**, *82*, 1620–1631.
(19) Asanov, A. N.; Nikic, D. B.; Oldham, P. B.; Wilson, W. W. In *8th International Conference on the Crystallization of Biological Macromolecules*, Sandestin, FL, 2000.

ments in efficiency of at least an order of magnitude in terms of protein and time consumption.

However, none of these techniques is capable of assaying protein self-association in a parallel format, which should lead to significant increases in efficiency. The efficiency of empirical crystallization screens is impressive and difficult to surpass since they are conducted in a parallel format with microliters of protein solution. Importantly, the basic premise of empirical crystallization screens, which is to detect whether given solution conditions will promote a crystalline phase separation, is relatively simple in comparison to the measurement of the corresponding thermodynamic properties.

We envision at least two approaches for assaying protein self-association in a parallel format. The first concept is to develop microfluidic versions of techniques that have already been established to measure B_{22}, which could be parallelized using lab-on-a-chip technologies. The most amenable techniques for measuring B_{22} for microfluidic applications are the chromatography based techniques, including self-interaction and size-exclusion chromatography. Indeed, a miniaturized version of self-interaction chromatography has recently been demonstrated, which currently represents the most efficient technique for measuring B_{22}.[20] However, challenges still remain in developing these techniques into quantitative, parallel microfluidic systems.

The other approach that we envision for assaying protein self-association in a parallel format is to use nanoparticles that possess optical properties that are dependent on the interparticle separation distance, which is the subject of this work. Motivation for the use of nanoparticles to assay weak protein interactions comes from pioneering work demonstrating that the separation-dependent optical properties of gold nanoparticles could be used to detect single base pair differences between DNA molecules.[21] Gold particles functionalized with DNA molecules were allowed to hybridize in solution, forming crosslinked networks of particles. The solutions could then be heated and single base-pair differences could be detected through differences in the melting temperature; DNA sequences encoding complete base pair registry melt at higher temperatures than those that do not.

It is not possible to use these concepts to investigate protein self-association, since most proteins are not thermostable, protein self-association is too weak to form stable cross-linked structures, and protein interactions are dependent on temperature. However, protein/gold conjugates have been used extensively in histochemistry to image cells using electron microscopy. Many reports have documented procedures for adsorbing proteins on the surface of gold nanoparticles (e.g., ref 22) and stabilizing them against aggregation (e.g., ref 23), which interestingly is often a problem. Several factors can influence the aggregation of protein/gold conjugates, but one potential driving force is protein self-association between proteins adsorbed on the nanoparticles. In this work, we seek to exploit the aggregation of protein/gold conjugates for assaying protein self-association and investigate its utility in the search for

solution conditions conducive to crystallization. We refer to this novel technique as self-interaction nanoparticle spectroscopy (SINS).

Experimental Section

Materials. Bovine serum albumin (BSA, A-7638) and ovalbumin (A-2512) were purchased from Sigma, and used as received. Gold chloride (G-4022), sodium phosphate (monobasic, S-0751), bis-tris (B-7535), magnesium chloride (M-2670), tannic acid (T-8406) and 5 nm gold particles (G-1402) were also obtained from Sigma. Ammonium sulfate (ACS grade, A702), sodium chloride (ACS grade, 5271) and tri-sodium citrate (BP327) were purchased from Fisher. Nochromix (C667) was obtained from Godax Laboratories, Inc.

Protein/Nanoparticle Conjugate Preparation. The gold nanoparticles (24 nm) were synthesized as described previously (concentration of 3×10^{-4} vol %).[24,25] However, smaller particles (5 nm) were purchased from Sigma and used for limited experiments. Protein was adsorbed on the gold particles at a concentration of 0.25−0.5 mg of protein per mL of total solution and a gold concentration of 2×10^{-4} vol %, unless otherwise noted, for 1 h. The protein−gold conjugates (PGCs), in solutions still containing the unbound protein, were added to plastic cuvettes containing various salt solutions of interest for crystallization in a ratio of 1:5. The final protein and gold concentrations were typically 50−100 μg/mL and 5×10^{-5} vol %, respectively.

Experiments were also conducted to evaluate the effect of the BSA concentration. The final BSA concentration was varied by adsorbing BSA at concentrations of 0.04, 0.25, 0.5 and 1 mg/mL, and a gold colloid concentration of 2×10^{-4} vol %. The samples were then diluted in various salt solutions to obtain final BSA concentrations of 8, 50, 100, and 200 μg/mL, and a final gold concentration of 5×10^{-5} vol %.

Aggregation Experiments. The PGCs were added to various salt solutions and their aggregation behavior was followed using a spectrophotometer by measuring the wavelength corresponding to the minimum in transmission; this wavelength is referred to as the plasmon mode. The plasmon mode for unaggregated gold nanoparticles used in this work corresponded to a wavelength of approximately 520−530 nm. The value of the plasmon mode for gold particles coated with protein in the absence of salt, λ_o, was used to normalize the position of the plasmon mode ($\lambda(t)$):

$$\frac{\Delta\lambda}{\lambda_o} = \frac{\lambda(t) - \lambda_o}{\lambda_o}$$

The measurements of the plasmon mode were conducted using a Perkin-Elmer Lambda 2 UV−vis spectrophotometer. All experiments were performed at 23 ± 2°C.

Dynamic Light Scattering. The size of the PGCs was measured by dynamic light scattering (DLS) at an angle of 90° using a Brookhaven light scattering apparatus equipped with an Ar-ion laser ($\lambda = 488$ nm) and a BI9000AT correlator. The samples were placed in an index matching fluid thermostated at 23 °C. The diffusion coefficient was obtained by fitting the autocorrelation function using the method of cumulants with a quadratic fit. The size of the particles was calculated using the Stokes−Einstein relation and assuming that the value of the viscosity was that of water. The count rate was greater than 10 kcps, and typically 10^6 counts were collected for evaluation of the size of the conjugates.

Transmission Electron Microscopy (TEM). TEM analysis of the PGCs was conducted by dispensing 5 μL of gold−BSA−salt solutions on ultrathin carbon grids (Electron Microscopy Sciences, CF300-Cu). After 20 min, the grids were washed with 5 μL of water, blotted to remove excessive water, and allowed to dry at room temperature.

(20) Garcia, C. G.; Hadley, D. G.; Wilson, W. W.; Henry, C. S. *Biotechnol. Prog.* **2003**, *19*, 1006−1010.
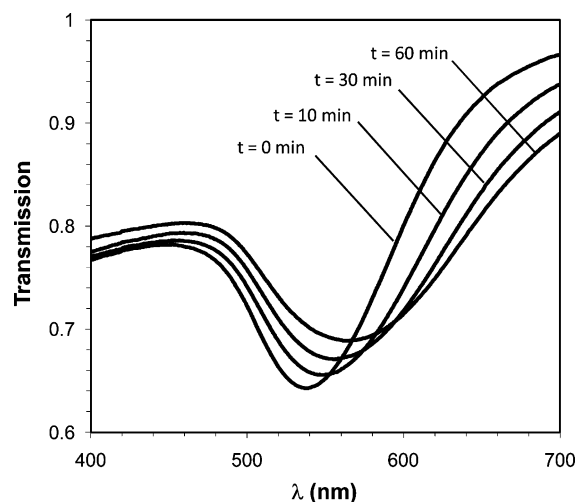(21) Elghanian, R.; Storhoff, J. J.; Mucic, R. C.; Letsinger, R. L.; Mirkin, C. A. *Science* **1997**, *277*, 1078−1081.
(22) Faulk, W. P.; Taylor, G. M. *Immunochemistry* **1971**, *8*, 1081.
(23) Geoghegan, W. D.; Ackerman, G. A. *J. Histochem. Cytochem.* **1977**, *25*, 1187−1200.

(24) Slot, J. W.; Geuze, H. J. *J. Cell Biol.* **1981**, *90*, 533−536.
(25) Slot, J. W.; Geuze, H. J. *Eur. J. Cell Biol.* **1985**, *38*, 87−93.

Figure 1. Transmission spectra for BSA/gold conjugates after incubation with ammonium sulfate at 6.3 M ionic strength and pH 6.2. The curves correspond to 0, 10, 30, and 60 min of aggregation, and the position of the minimum red-shifts as a function of time.

Electron micrographs were collected using a Tecnai 12 TEM at 120 kV and recorded using a Gatan 791 MSC camera.

Results

**Characterization of BSA/Gold Nanoparticle Aggregation.** The addition of BSA/gold conjugates to certain salt solutions led to a change in their optical properties, which were characterized in terms of the plasmon shift. A sample series of spectra as a function of time for BSA/gold conjugates at pH 6.2 and 6.3 M ammonium sulfate ionic strength is shown in Figure 1. The plasmon mode shifted to larger wavelengths, and the fractional transmittance increased, as a function of time. The color of the gold solution also changed from pink to purple as a function of time.

The BSA/gold conjugates were characterized in more detail using dynamic light scattering (DLS). The diameter of the unaggregated conjugates was estimated from DLS to be 37 nm as compared to 24 nm for the bare gold nanoparticles, corresponding to approximately a monolayer of adsorbed BSA using an average BSA diameter (5.4 nm), as observed previously.[26] Kinetic data for the effective size of the BSA/gold aggregates formed at 4.5, 6.3 and 7.5 M ammonium sulfate ionic strength and pH 6.2 are shown in Figure 2A. The corresponding data for the plasmon shift as a function of ionic strength and time are shown in Figure 2B. The DLS measurements indicate that the aggregates are largest at the highest ionic strength (7.5 M), but the plasmon shift is largest at intermediate ionic strength (6.3 M). Both the plasmon shift and the effective size of the aggregates show roughly power-law dependence on time.

In Figure 3, the positions of the plasmon mode for experiments similar to those shown in Figure 2 are plotted as a function of ionic strength at 20, 30, and 60 min. The curves indicate three regimes: the plasmon shift is near zero and independent of electrolyte concentration at low ionic strength, it increases at moderate ionic strength, and it decreases at high ionic strength to values near zero. The plasmon shift displays a maximum at 6.3 M ionic strength, and the position of the maximum is relatively invariant as a function of time. Measure-

(26) Deroe, C.; Courtoy, P. J.; Baudhuin, P. *J. Histochem. Cytochem.* **1987**, *35*, 1191−1198.
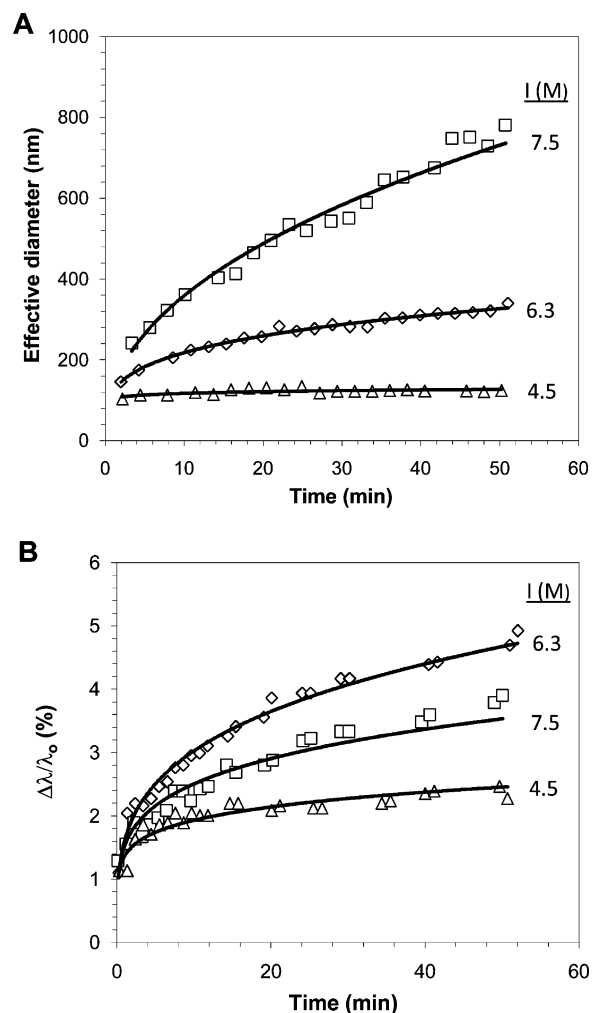
Figure 2. Kinetics of BSA/gold aggregation at pH 6.2 and 4.5 (△), 6.3 (◇), and 7.5 (□) M ammonium sulfate ionic strength characterized by measurements of (A) the effective diameter and (B) the plasmon shift. The final gold and BSA concentrations were 9×10^{-5} vol % and 0.15 mg/mL, respectively, and the size of the gold nanoparticles was 24 nm. The trend lines are power law fits.
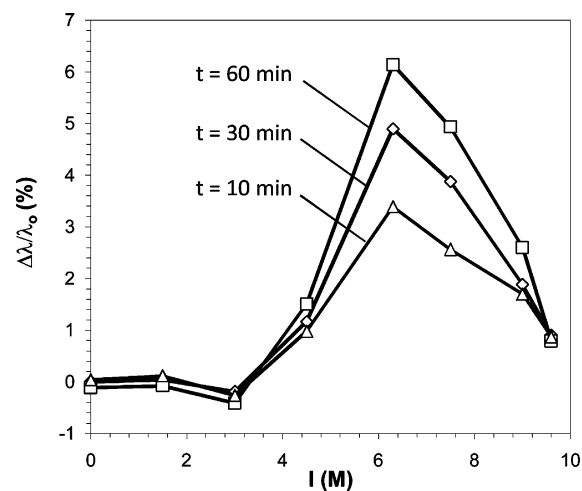
Figure 3. Normalized plasmon shift as a function of the ionic strength for BSA/gold conjugates after 10 (△), 30 (◇), and 60 (□) minutes of incubation with ammonium sulfate. The final gold and BSA concentrations were 5×10^{-5} vol % and 50 μg/mL, respectively.

ments performed at a larger number of ionic strength values revealed that the maximum was typically between 6.0 and 6.3
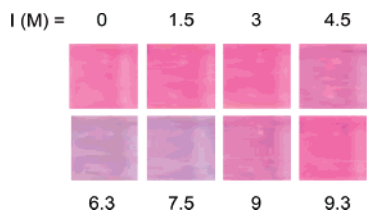
Figure 4. Optical images of the BSA/gold solutions after approximately 2 h of incubation with ammonium sulfate at (top row, left to right) 0, 1.5, 3, 4.5, and (bottom row, left to right) 6.3, 7.5, 9 and 9.6 M ionic strength and pH 6.2. The images are of the samples used to measure the plasmon shift in Figure 3.

M ionic strength for this system (data not shown). These results were reproducible, but the maximum was observed to appear at lower ionic strengths (4.5 M) if the gold colloid was aged for more than 1 month after it was synthesized (data not shown).

Optical images of the BSA/gold samples used in Figure 3, taken through the top openings of the plastic cuvettes used in the spectrophotometer after approximately 2 h, are shown in Figure 4. As the ionic strength is increased, the gold solution changes color from pink to purple to pink. The solutions at moderate to high ionic strength (>3M) formed visible aggregates after several hours that settled to the bottom of the cuvettes. At moderate ionic strength (4.5−7.5 M ionic strength), the aggregates were dense and purple, whereas at high ionic strength (>7.5 M) they were pink and fluffy.

TEM images of BSA−gold conjugates (Figure 5) revealed that the interparticle spacings were strongly dependent on the ammonium sulfate concentration. The gold particles in the presence of 0 (Figure 5A) and 9.6 (Figure 5C) M ammonium sulfate ionic strength were well separated, while the particles at 6.3 M (Figure 5B) were aggregated and in close proximity. These differences were dramatic since few aggregated particles were observed in the 0 and 9.6 M samples or well-separated particles in the 6.3 M samples.

Comparison of the Plasmon Mode with the Osmotic Second Virial Coefficient. Osmotic second virial coefficients for BSA (in the absence of gold nanoparticles) at pH 6.2[27] are shown in Figure 6, along with the normalized plasmon shift for BSA/gold conjugates after 60 min of incubation with various concentrations of ammonium sulfate. The B_{22} values are positive, corresponding to repulsive protein interactions, below 4 M ionic strength, and the plasmon shift is close to zero. At moderate ionic strength (4−7 M) the B_{22} values are relatively small and negative, corresponding to weakly attractive protein interactions, and the plasmon shift increases as the protein interactions become more attractive. The virial coefficient value at 6.3 M ionic strength lies inside the crystallization slot, and corresponds to the maximum shift of the plasmon mode. At high ionic

strength (7.5 M), the value of B_{22} lies below the crystallization slot, which corresponds to strongly attractive protein interactions, and the relative plasmon shift decreases at ionic strengths equal to or greater than 7.5 M.

A comparison of the second virial coefficient[28,29] and the plasmon shift for BSA in sodium chloride solutions at pH 7 is shown in Figure 7. The virial coefficient is a weak function of the ionic strength up to 4 M ionic strength, and the plasmon shift remains close to zero over this full range of ionic strength values.

In Figure 8, the values of the second virial coefficient[30] and the positions of the plasmon mode for ovalbumin are shown at pH 6 as a function of the ammonium sulfate ionic strength. At relatively low ionic strength (<3 M), the B_{22} values are slightly negative, corresponding to very weak attractive interactions, and the plasmon shift is near zero. At ionic strength values between about 3 and 4.5 M, the B_{22} values lie inside the crystallization slot, which corresponds to weakly attractive protein interactions, and the plasmon mode shifts to larger values as a function of ionic strength. The virial coefficient value at 4.5 M ionic strength lies in the middle of the crystallization slot, and this ionic strength corresponds to the maximum shift of the plasmon mode. At high ionic strength (>5 M), the virial coefficient value lies below the crystallization slot, corresponding to strongly attractive protein interactions, and the plasmon mode shifts to lower values as a function of ionic strength.

Figure 9 illustrates a similar comparison for ovalbumin between B_{22} values[30] and the plasmon shift at pH 7 as a function of the magnesium chloride ionic strength. The virial coefficients are a weak function of ionic strength and are slightly negative or positive, which corresponds to very weakly attractive or repulsive protein interactions, respectively. The plasmon shift is a weak function of ionic strength as well, and the value of the normalized shift is close to zero.

Sensitivity of the Plasmon Mode to Experimental Parameters. The effect of the final BSA concentration on the plasmon shift is shown in Figure 10. Above 4.5 M ionic strength, the magnitude of the plasmon shift is greater as the BSA concentration is decreased. Moreover, the relative trend of the plasmon shift as a function of ionic strength is the same for the various BSA concentrations.

The results in Figure 11 show the effect of the size of the gold nanoparticles on the plasmon shift. The magnitude of the plasmon shift is greater for the 24 nm particles than for the 5 nm particles. Further, the overall trends are similar for particles of both sizes as a function of ionic strength.
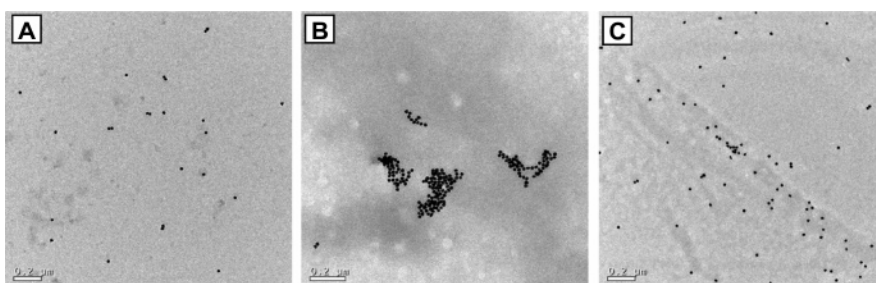
Figure 5. Transmission electron microscopy images of BSA/gold conjugates at pH 6.2 and (a) 0 M, (b) 6.3 M, and (c) 9.6 M ammonium sulfate ionic strength. The scale bars are 200 nm.
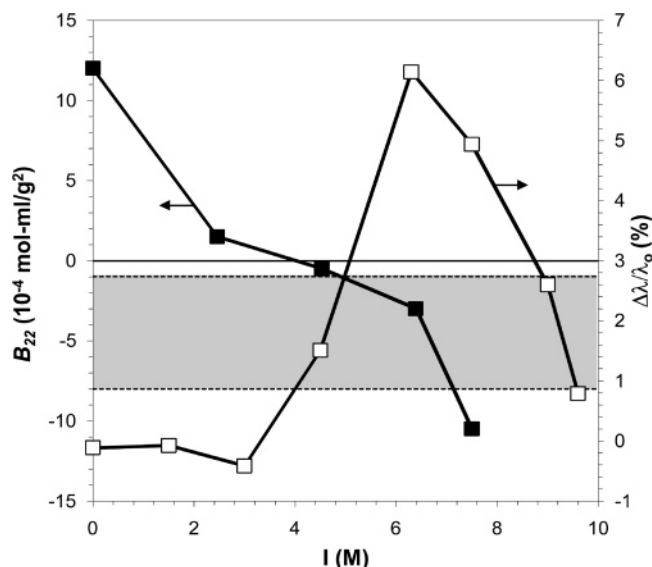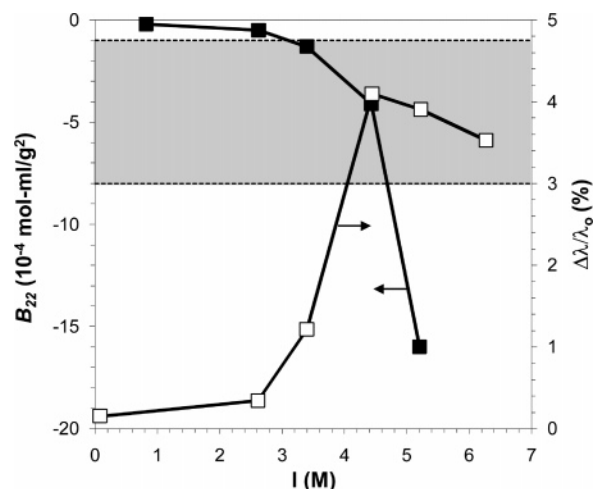
Figure 6. Osmotic second virial coefficients for BSA at pH 6.2 and 50 mM sodium phosphate as a function of the ammonium sulfate ionic strength (■, ref 27), and the plasmon shift for BSA/gold conjugates after 60 min of incubation with ammonium sulfate (□). The final gold and BSA concentrations were 5×10^{-5} vol % and 50 μg/ mL, respectively. The shaded region corresponds to the crystallization slot.
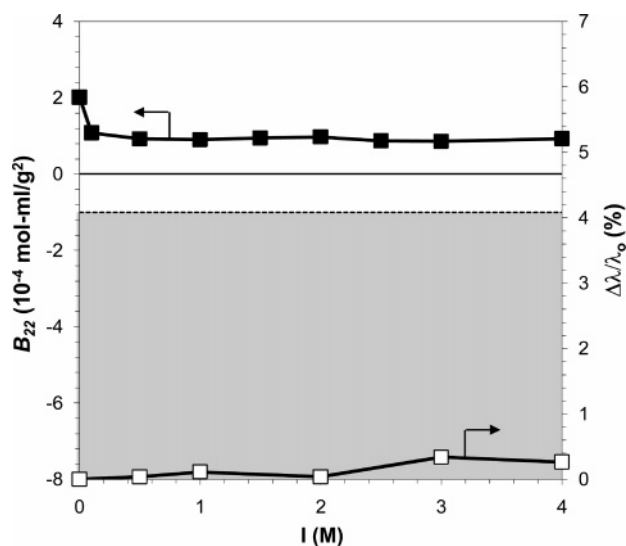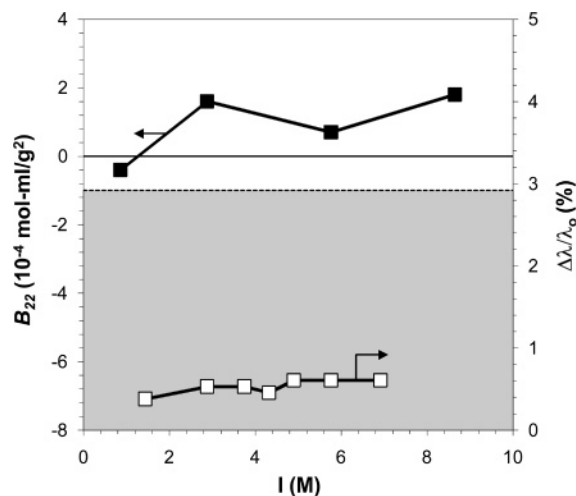

Figure 7. Osmotic second virial coefficients for BSA at pH 7 and 10 mM bis-tris as a function of the sodium chloride ionic strength (■, refs 28–29), and the plasmon shift for BSA/gold conjugates after 60 min of incubation with sodium chloride (□). The final gold and BSA concentrations were 5×10^{-5} vol % and 50 μg/mL, respectively. The shaded region corresponds to the crystallization slot.

Discussion

Relationship between the Osmotic Second Virial Coefficient and the Plasmon Mode. A significant finding in this work is that values of the osmotic second virial coefficient that lie inside the crystallization slot correspond to a maximum shift of the plasmon mode as a function of ionic strength. Indeed, published crystallization conditions for BSA correspond to those that were observed in Figure 3 to lead to a maximum shift of the plasmon mode (pH 6.2, 6.3 M ammonium sulfate ionic strength).[27] Conditions that have been shown to lead to ovalbumin crystallization (pH 6.2, 4.5 M ammonium sulfate ionic strength, 30 °C)[31] are very similar to those found to lead to the maximum shift of the plasmon mode (pH 6, 4.5 M

Figure 8. Osmotic second virial coefficients for ovalbumin at pH 6 as a function of the ammonium sulfate ionic strength (■, ref 30), and the plasmon shift for ovalbumin/gold conjugates after 60 min of incubation with ammonium sulfate (□). The final gold and ovalbumin concentrations were 5×10^{-5} vol % and 0.1 mg/mL. The shaded region corresponds to the crystallization slot.

Figure 9. Osmotic second virial coefficients for ovalbumin at pH 7 as a function of the magnesium chloride ionic strength (■, ref 30), and the plasmon shift for ovalbumin/gold conjugates after 60 min of incubation with magnesium chloride (□). The final gold and ovalbumin concentrations were 5×10^{-5} vol % and 0.1 mg/ mL. The shaded region corresponds to the crystallization slot.

ammonium sulfate ionic strength, 23 °C). This remarkable correlation suggests that this assay may be useful for screening for solution conditions that promote crystallization for proteins that have not been crystallized previously.

Why does the plasmon mode for the PGCs show a maximum shift for weakly attractive protein interactions that are ideal for crystallization? This behavior can be explained by the schematic diagram in Figure 12. At relatively low ammonium sulfate ionic strength, BSA and ovalbumin interactions are repulsive and very weakly attractive, respectively. Therefore, the proteins on the

(27) Asanov, A. N.; DeLucas, L. J.; Oldham, P. B.; Wilson, W. W. *J. Colloid Interface Sci.* **1997**, *196*, 62–73.
(28) Tessier, P. M.; Lenhoff, A. M. *Curr. Opin. Biotech.* **2003**, *14*, 512–516.
(29) Tessier, P. M.; Vandrey, S. D.; Berger, B. W.; Pazhianur, R.; Sandler, S. I.; Lenhoff, A. M. *Acta Crystallogr. D* **2002**, *58*, 1531–1535.
(30) Curtis, R. A.; Ulrich, J.; Montaser, A.; Prausnitz, J. M.; Blanch, H. W. *Biotechnol. Bioeng.* **2002**, *79*, 367–380.
(31) Judge, R. A.; Johns, M. R.; White, E. T. *J. Chem. Eng. Data* **1996**, *41*, 422–424.
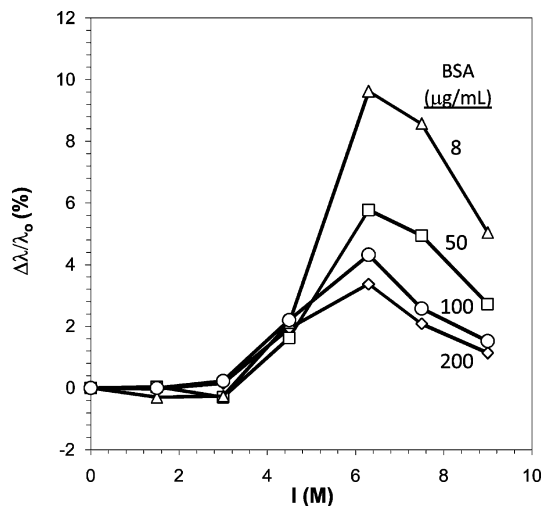
Figure 10. Effect of the BSA concentration on the plasmon shift as a function of the ammonium sulfate ionic strength at pH 6.2 and 50 mM sodium phosphate. The BSA concentrations were 0.008 ($\triangle$), 0.05 ($\square$), 0.1 ($\bigcirc$), and 0.2 ($\diamond$) mg/mL, and the gold concentration was 5×10^{-5} vol %.
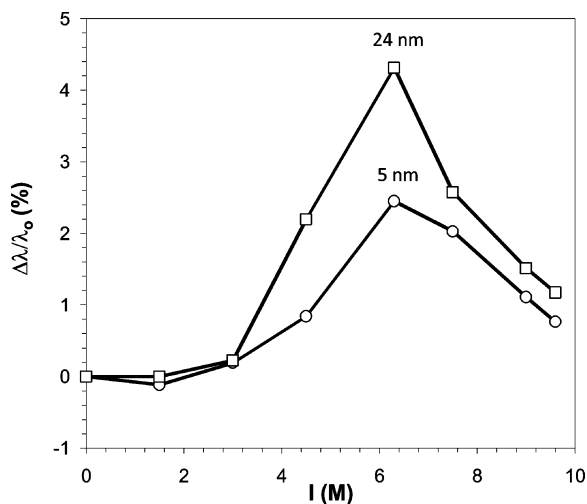
Figure 11. Effect of nanoparticle size on the plasmon shift for BSA/gold conjugates at pH 6.2 as a function of the ionic strength after 60 min of incubation with ammonium sulfate. The size of the gold particles was 5 ($\bigcirc$) and 24 ($\square$) nm, the BSA concentration was 0.1 mg/mL, and the gold concentration was 5×10^{-5} vol %.

surface of nearby gold nanoparticles repel each other or associate very weakly, which does not lead to aggregation of the PGCs (Figure 12, left image). At moderate ammonium sulfate ionic strength, the protein interactions are weakly attractive and the

virial coefficient values lie inside the crystallization slot, and therefore the proteins on the surface of the nanoparticles attract each other and aggregate (Figure 12, center image). Importantly, the position of the plasmon mode shifts to larger wavelengths more sharply as the degree of attraction between the proteins is increased.

The behavior at high ammonium sulfate ionic strength appears to be due to a competitive aggregation process between protein in solution and protein adsorbed on the surface of the gold particles (Figure 12, right image). Due to the strong protein interactions at high ionic strength, protein in solution is attracted to protein on the surface of the PGCs and aggregates on the surface of the PGCs before the PGCs can self-associate. Therefore, when the PGCs aggregate with each other, there are multiple layers of protein separating the gold nanoparticles and, thus, the plasmon shift is reduced.

Support for this competitive aggregation mechanism at high ammonium sulfate concentrations comes from three lines of reasoning. First, the TEM analysis of the BSA PGCs showed that the close interparticle spacings were only observed at moderate ionic strength (6.3 M), whereas the particles were well spaced at both low (0 M) and high (9.6 M) ammonium sulfate ionic strength. Dynamic light scattering analysis confirmed that at high ionic strength the large interparticle spacings are not due to a lack of aggregation since PGC aggregate size increased as a function of ionic strength (Figure 2A). Second, visual inspection of the PGC aggregates revealed that at moderate ionic strength (6.3 M), the aggregates were dense, similar to the appearance of the gold aggregates in the absence of protein, and purple. However, the aggregates formed at high ionic strength (9.6 M) were fluffy and pink, and could be easily sheared and dispersed temporarily, unlike those formed at moderate ionic strength (6.3 M). This also suggests that more protein is incorporated between the gold particles in the aggregates at high ionic strength.

The third line of reasoning for the competitive aggregation mechanism is based on factors that influence the plasmon shift for metallic nanoparticles, including the refractive index of the surrounding medium, which can be influenced by the solvent and adsorbed molecules, and the average separation distance of the nanoparticles.[32] As the refractive index of the surrounding medium increases, the plasmon mode shifts to higher wavelengths. Indeed, this was observed when BSA and ovalbumin were adsorbed on the surface of the gold nanoparticles since the plasmon mode red-shifted about ~5 nm or 1%, which agrees
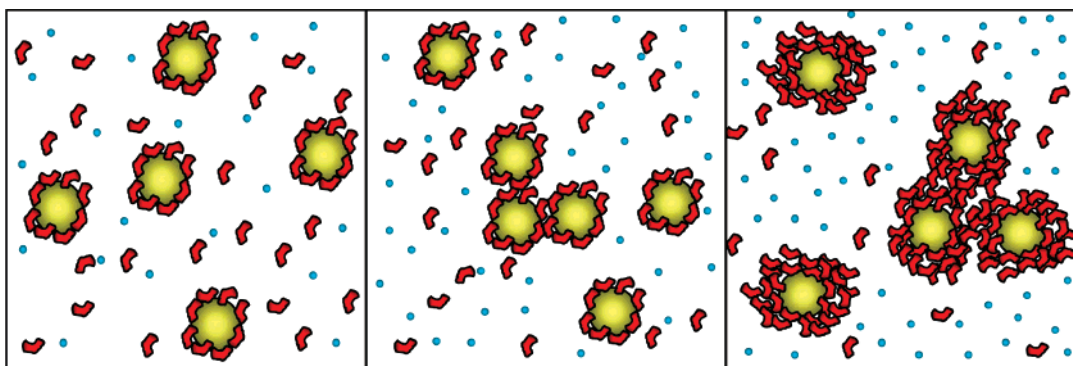
Figure 12. Schematic diagram of the protein/gold conjugates at solution conditions corresponding to protein interactions that are repulsive or very weakly attractive (left), weakly attractive (center), and strongly attractive (right).

with previous observations for the adsorption of gelatin on gold nanoparticles.[33] Although additives (e.g., salt) may also change the refractive index of the medium, it was confirmed that this has a negligible effect on the plasmon shift (data not shown).

As the separation of the nanoparticles decreases, the plasmon mode shifts to larger wavelengths due to excitation of resonance modes that exist along the longitudinal axis between two particles in close proximity.[32] The magnitude of the plasmon shift due to interparticle proximity for two particles in contact can be >100 nm or 20% and therefore is likely a more significant contribution than the altered refractive index of the corona surrounding the nanoparticles in the aggregation experiments. Both multilayer adsorption of protein on the nanoparticle surface and aggregation of the nanoparticles will separately increase the plasmon shift. However, multilayer protein adsorption on the PGCs, and subsequent aggregation of the PGCs, can explain the relative decrease in the shift of the plasmon mode at very high ionic strength, supporting the physical mechanism illustrated in Figure 12.

Importantly, PGC aggregation was not seen in the control experiments in Figures 7 and 9 for BSA and ovalbumin in salts (sodium chloride and magnesium chloride) that do not lead to significant attractive self-association. This is also consistent with the ineffectiveness of these salts in crystallizing ovalbumin or BSA. The high stability of the PGCs in sodium chloride and magnesium chloride is in stark contrast to the behavior of the gold nanoparticles in the absence of adsorbed protein; unconjugated gold nanoparticles are remarkably unstable, and can aggregate at millimolar concentrations of electrolyte. Therefore, it is clear that the adsorbed protein on the surface of the nanoparticles exerts a significant influence on the aggregation behavior of the gold colloid.

Implications for Protein Crystallization. The results of this work provide proof of the concept of using nanoparticles to identify solution conditions that correspond to B_{22} values inside the crystallization slot, i.e., conditions that have been shown to be conducive to protein crystallization. An important question is whether this technique will be useful for proteins that possess different physical and chemical properties. BSA and ovalbumin are both acidic proteins, and they were adsorbed and studied at pH values above their pI, where they possess a net negative charge. Since gold particles are negatively charged, the addition of positively charged proteins could lead to nonspecific aggregation between the oppositely charged particles. Indeed, the addition of lysozyme (pI 11) at neutral pH resulted in an immediate color change of the gold colloid solution, indicating that aggregation had occurred, even though the lysozyme interactions are repulsive at conditions of low ionic strength (<0.1 M).[4] To overcome this problem, the nanoparticle surface will need to be modified with, for example, self-assembled monolayers before subsequent immobilization of the protein molecules.

It is also important to consider how this technique could be implemented in practice. Since the plasmon shift is dependent on the protein and gold concentration, the ratio of the protein size to that of the gold particles, and the aggregation time, it is not possible to define a specific range of values of the plasmon shift that are conducive to crystallization as has been done for B_{22}. However, the qualitative nature of this method must be contrasted with its remarkable efficiency in terms of time and protein consumption, and the ease of parallelization. For example, the BSA experiments in Figure 10 were performed at a concentration of 8 μg/mL, which is about 3 orders of magnitude lower than the protein concentrations required currently to measure the second virial coefficient. Also, the samples were prepared and characterized in approximately 2 h. The length of time required is determined largely by the time required for adsorption of the protein, and subsequent association of the PGCs in the presence of solution additives. Therefore, the time required to characterize the samples depends only weakly on the number of samples, especially if visual detection of the color change is utilized.

There are important advantages of SINS relative to empirical crystallization screens that should also be emphasized. Crystallization screens that seek to detect a phase change must be conducted above the solubility limit, while detection of the aggregation state of PGCs was conducted at protein concentrations well below the solubility limit of BSA and ovalbumin. Also, the crystallization of proteins can require days to months, while the protein/gold aggregation experiments were conducted and analyzed in a few hours. Therefore, it appears that increases in efficiency relative to empirical crystallization screens should be possible.

Conclusions

The optical properties of PGCs have, for the first time, been connected to the degree of protein self-association. For some solution conditions, a competitive aggregation process exists between protein in solution and the PGCs, and the PGCs themselves. This competition provides remarkable discrimination of conditions that correspond to negative B_{22} values that lie inside the crystallization slot. Self-interaction nanoparticle spectroscopy is also unique among techniques available for probing protein self-association in being a parallel method that requires little instrumentation, and detection can be done by eye. A major accomplishment of this work is the development of a method that may rival empirical crystallization screens in terms of time and protein consumption. Future work will focus on extending this method to investigate self-association of proteins that have not been crystallized previously, such as membrane proteins.

JA077624Q

(32) Kreibig, U.; Vollmer, M. *Optical Properties of Metal Clusters*; Springer-Verlag: New York, 1995.
(33) Eck, D.; Helm, C. A.; Wagner, N. J.; Vaynberg, K. A. *Langmuir* **2001**, *17*, 957−960.